JOURNAL OF MATERIALS SCIENCE 30 (1995) 3149–3154

Characterization of the paste–aggregate interfacial transition zone surface roughness and its relationship to the fracture toughness of concrete

D. ZAMPINI, H. M. JENNINGS, S. P. SHAH
NSF Center for Advanced Cement-Based Materials, Department of Civil Engineering, Northwestern University Evanston, IL 60208, USA

Notched concrete beams containing varying amounts of pea gravel aggregate were tested under three-point bend, and their fracture toughness determined. The roughness of the region near the interface between the cement paste and the aggregate was evaluated by digitizing images from a confocal tandem scanning microscope. The average roughness of the paste was found to be related to the fracture parameters K_{IC} (critical stress intensity factor) and Δa_c (critical crack extension), as determined by the two-parameter fracture model. The roughness in the proximity of the paste–aggregate interface was generally higher than that of the paste far from the aggregate, and it decreased with the distance from the aggregate. This study indicates that aggregate particles increase the toughness of the cement paste portion of concrete, and that this is an important mechanism for toughening concrete.

1. Introduction

Studies related to the characterization of the process of fracture in cement-based materials [1, 2] have demonstrated that, in general, the fracture toughness of concrete is higher than that of mortar, which is higher than that of paste. However, the trend does not hold for tensile strength, and, in general, this property has smaller values in concrete than in mortar, and both are smaller than in paste. Therefore, a cement-based material that possesses high strength but low fracture toughness (paste) is more brittle than a material that exhibits low strength and high fracture toughness (concrete). The increased fracture toughness in concrete has been attributed to the presence of aggregate particles which toughen the material by interfering with crack propagation.

Generally, the resistance to crack propagation provided by aggregate particles may be explained by several possible mechanisms associated with the formation of a fracture process zone (FPZ). One mechanism, proposed by Kachanov [3], is that microcracks that are formed by growth at flaws (voids, porosity, shrinkage cracks) around the crack tip, shield or otherwise cause the reduction of stress at the crack tip. Faber and Evans [4] showed that cracks have a tendency to deflect around strong aggregate particles or along weak interfacial regions. Another proposed mechanism invokes crack bridging [5], which provides closing stresses behind the crack tip. Also, when the fracture surface is rough, interlocking of the crack surfaces consumes energy through friction [6], and this may be an important mechanism.

The proposed mechanisms for the toughening of concrete, however, do not explicitly examine the effects that the paste–aggregate interface has on fracture. Because concrete is weaker than paste, its paste–aggregate interfaces have been assumed to be relatively weak.

Probably the first observation of the paste–aggregate interfacial zone was reported by Faran in 1956 [7, 8]. Since then, investigations have revealed the chemical [9–14], mechanical [14–16], and electrical properties [17] of the paste–aggregate interfacial region. These studies have been indirect for they have been aimed primarily at the characterization of the properties of the interfacial region, but the mechanisms by which the aggregate and its associated interfacial zone contribute to the production of tougher concrete are far from being completely understood.

A microstructural feature that is indicative of the toughness of a material is the roughness of fracture surfaces: high roughness is associated with a tough material. Visual observation of the fracture surfaces of concrete reveals the influence that aggregate particles have on roughness (see Fig. 1): increasing the amount of aggregate increases the roughness of the fracture surfaces. Studies carried out by Lange *et al.* [18] showed, quantitatively, that the roughness of mortar surfaces is correlated with fracture toughness. In this paper, the influence of the roughness of the paste portion of concrete is studied and related to toughness. Furthermore, the roughness is correlated with distance from the aggregate particles. This study is aimed at refining our understanding of the

0022–2461

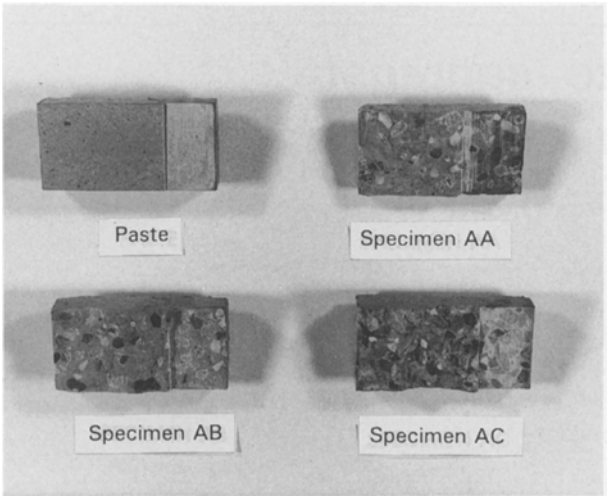

Figure 1 Sawn-off portions of the fracture surfaces that were used for analysis under the confocal microscope.

mechanisms involved in toughening of concrete. Specifically, the roughness of the paste portion is studied to determine whether or not the paste is toughened by the presence of aggregate particles.

2. Experimental procedure

2.1. Design of experiments

Beams were cast using concrete made of a type I cement and pea gravel aggregate as constituents. The pea gravel had a water absorption value of 1.33% (air dry to saturated surface dry (SSD) state), and was sieved so that 100% of the aggregate passed through a no. 4 sieve (4.75 mm opening) and 100% was retained in no. 8 sieve (2.36 mm opening). Thus the aggregate had a narrow size distribution. Four series of specimens were cast, including control specimens consisting solely of paste. All specimens had a water to cement ratio of 0.45. Each series of specimens (C, AA, AB, and AC) contained a particular amount of aggregate (0.0, 0.50, 1.0, and 2.5 times the weight of cement). This design resulted in concrete specimens having the following water to cement to aggregate ratio: C 0.45:1.0:0.0, AA 0.45:1.0:0.5, AB 0.45:1.0:1.0, AC 0.45:1.0:2.5. Each batch was cast into six beams in plexi-glass moulds having the dimensions 9 in × 3 in × 1 in (~ 22.9 cm × 7.6 cm × 2.5 cm; span × height × thickness). The beams were cured in lime water for 28 days prior to testing. A summary of batch design is given in Table I.

2.2. Mechanical testing

Mechanical testing of notched beams was accomplished using three-point bend, controlled by crack mouth opening displacement (CMOD). A notch was cut with a band saw. The dimensions and geometry of the beams are shown in Fig. 2. The beams were tested in accordance with the procedure specified by RILEM's "Determination of Fracture Parameters of Plain Concrete using Three-Point Bend Tests" [19], which is based on the two-parameter fracture model (TPFM) of Jenq and Shah [20]. Fracture parameters were obtained and related to the roughness of the paste. The fracture surfaces of the beams were sawn off to facilitate observation under the confocal microscope (see Fig. 1).

Concrete is a quasi-brittle material, and therefore conventional linear-elastic fracture mechanics cannot be applied to the study of the fracture process, which initially experiences slow, non-linear crack growth (a fracture process zone). In this study, the experimentally derived two-parameter fracture model (TPFM) is employed to evaluate fracture parameters (specifically K_{IC} and Δa_c). A typical load versus CMOD curve derived from the mechanical testing and beam loading configuration is shown in Fig. 3. Compliances for the loading, C_i, and unloading, C_u, portions of the curves and the peak load, P_{max}, are measured from the graph. The data from the curves and the parameters associated with the geometry of the beam are used to calculate the critical stress intensity factor, K_{IC}, critical crack tip opening displacement, $CTOD_c$, critical effective crack length, a_c, and critical effective crack extension, Δa_c, where $\Delta a_c = a_c - a_0$, and a_0 is the initial notch length. It is important to keep in mind that Δa_c is an estimate of the actual critical crack length extension. Crack propagation, and therefore Δa_c, or a_c, is more accurately represented by a model that enables prediction of a three-dimensional crack profile.

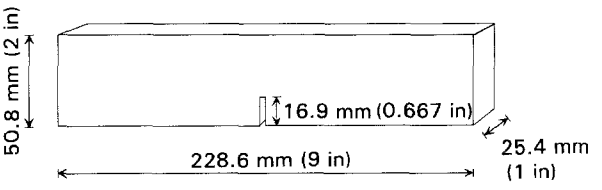

Figure 2 Geometry and dimensions of the beams tested under three-point bend.

TABLE I Summary of the batch design of notched beam specimens containing pea gravel aggregate (W = water, C = cement, A = aggregate)

	Aggregate			
Specimen	Type	Size (mm)	Amount	W:C:A
C	None	None	None	0.45:1.0:0.0
AA	Pea gravel	4.75–2.36	0.5 × wt of C	0.45:1.0:0.5
AB	Pea gravel	4.75–2.36	1.0 × wt of C	0.45:1.0:1.0
AC	Pea gravel	4.75–2.36	2.5 × wt of C	0.45:1.0:2.5

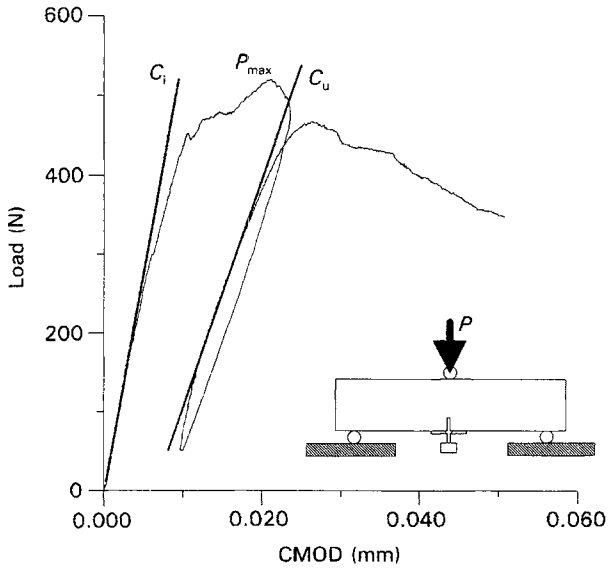

Figure 3 A typical load versus CMOD curve as obtained from three-point bend tests. Information obtained for the graph (C_u, C_i, P_{max}) is used to calculate fracture parameters from the TPFM.

2.3. Confocal microscopy

The fracture surfaces were reconstructed using the Confocal Tandem Scanning Reflected Light Microscope, by a method modified from Lange *et al.* [18, 21]. A two-dimensional topographic map of the surface was formed by sectioning the surface. Three-dimensional micrographs of the fracture surface were constructed at a magnification of 600×, making it possible to focus solely on the paste regions, and more specifically on the interfacial zone next to the aggregate particle. This magnification resulted in an image with dimensions of 146 μm × 137 μm, consisting of a 512 pixel × 480 pixel picture, with each pixel measuring 0.285 μm on a side. The stage supporting the fracture surface was moved from the highest point on the surface to the deepest point in 4 μm increments. Variation in depth (*z*-height) ranged from 50–160 μm, depending on the type of specimen. A typical topographic image is shown in Fig. 4, and a three-dimensional representation of the surface (produced from the topographic image) is shown in Fig. 5.

The surface area is computed by summing the area of triangles formed by connecting the *z*-height of adjacent pixel points, see Fig. 6. Roughness is evaluated by dividing the actual surface area by the nominal projected area as

$$RN = \frac{\text{actual surface area}}{\text{nominal surface area}} = \frac{\sum A_s}{\sum A_n} \quad (1)$$

where RN is the roughness number [17, 20].

In this research, the computer program was modified so that RN on areas smaller than the 146 μm × 137 μm image could be attained. Thus start and end values for the *y* coordinate are specified, and the image is divided into subregions. The size of the rectangular subregions are chosen to have the dimensions of 146 μm × 32 μm.

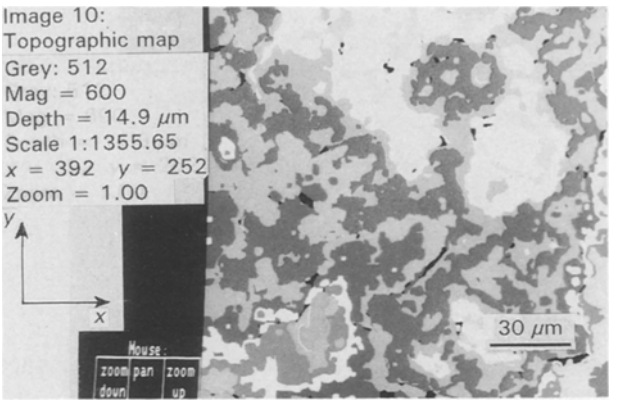

Figure 4 A typical two-dimensional, digitized, topographic image of the paste surface.

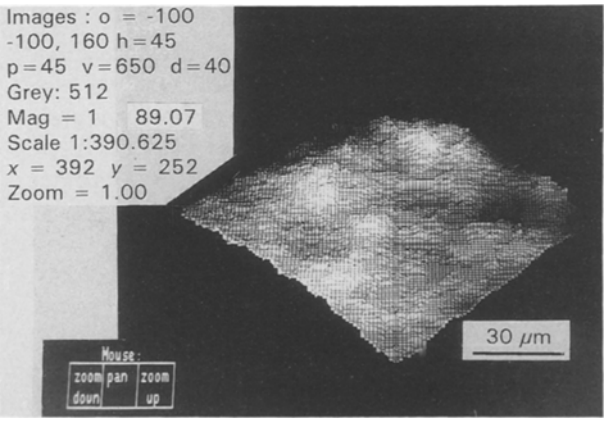

Figure 5 A typical three-dimensional image of the paste fracture surface. The surface features are reproduced using information from the topographic image.

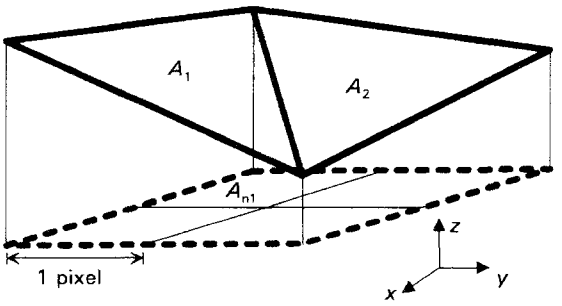

$$RN = \frac{\Sigma (A_1 + A_2 + \ldots + A_i)}{\Sigma (A_{n1} + A_{n2} + \ldots + A_{ni})} = \frac{\Sigma A_s}{\Sigma A_n}$$

Figure 6 Schematic diagram of the method by which roughness number, RN, is computed from the topographic images [18, 21].

3. Results and discussion

3.1. Characterization of the surface roughness of the paste

This paper reports the results of the determination of the paste roughness for the various specimens. Also, the paste roughness was evaluated as a function of the distance from aggregate particles. Initially, for each series of specimens (C, AA, AB, and AC), the RN of the

TABLE II Roughness numbers, *RN*, of paste surface computed without regard for the distance from the aggregate particle

Specimen	Roughness number, *RN*
C	3.27
AA	3.58
AB	3.65
AC	4.35

paste was evaluated by computing the average of the roughness values obtained for ten different regions on the fracture surface. In this preliminary analysis, no attempts were made to relate the region of the surface to its relative distance from the aggregate. The results are summarized in Table II. The surface roughness of the paste increased with increased volume of aggregate, which ranged from 0–2.5 times the volume of paste.

Careful correlation of the surface roughness to the location of the area being analysed lead to the observation that the roughness near the aggregate is greater than the roughness in regions away from the aggregate. This trend in *RN* was then reinforced by comparing micrographs such as those in Fig. 7a (which is an image of a region immediately surrounding the aggregate) with Fig. 7b (which is an image representative of a region removed and distant from the aggregate).

In order to evaluate the relationship between *RN* and distance from the aggregate, three topographic images were constructed for regions adjacent to one another in a sequence moving away from the interfacial zone. Each topographic image was divided into four subregions. The roughness number for each subregion is plotted against distance from the aggregate in Fig. 8. Generally, roughness decreases continuously as the distance from the aggregate increases.

Comparison of the results in Table II with Fig. 8 reveals some interesting trends. The *RN* for the control paste is about 3.27 (see Table II). This is the value which is approached in the other pastes at distances from the aggregate greater than about 100 μm (see Fig. 8). If roughness, as opposed to porosity [22] or microhardness [23], is the microstructural parameter used to define the transition zone (the transition/interfacial zone is defined as the distance from the aggregate surface where the *RN* begins to level off and approach the *RN* value of the control paste), then the observed size is larger than the 40–50 μm dimension often reported [9, 22]. However, moving closer to the aggregate, in Fig. 8, the *RN* converges on a value between 4.3 and 4.5 which is close to the *RN* (4.35) obtained from the initial analysis of the paste of the specimen with the highest aggregate content (specimen AC). On a random basis, the probability of examining the interfacial region in specimen AC is higher than in the other specimens, and therefore the *RN* values are close to those encountered at the interface.

Assuming a close-pack configuration of spherical particles having a coordination number of 12, calculations of the theoretical spacing between aggregate particles were carried out. This specific arrangement

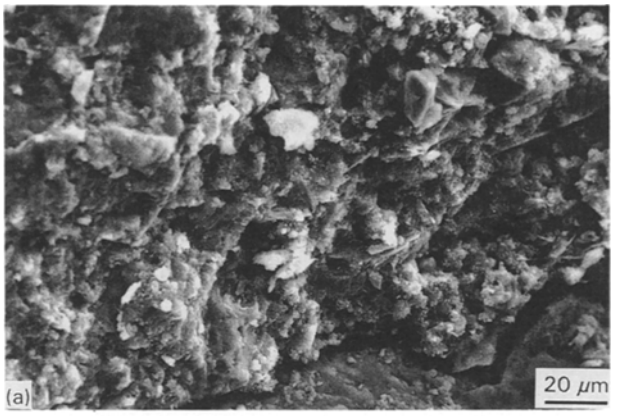

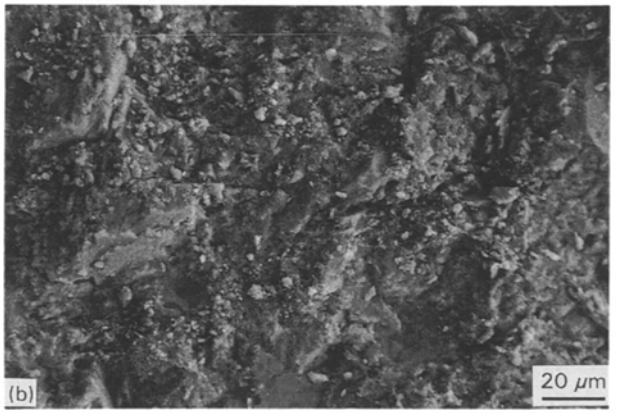

Figure 7 Back-scattered electron (BSE) micrographs of (a) a region near the aggregate particle, and (b) a region of the paste that is distant from the aggregate particle.

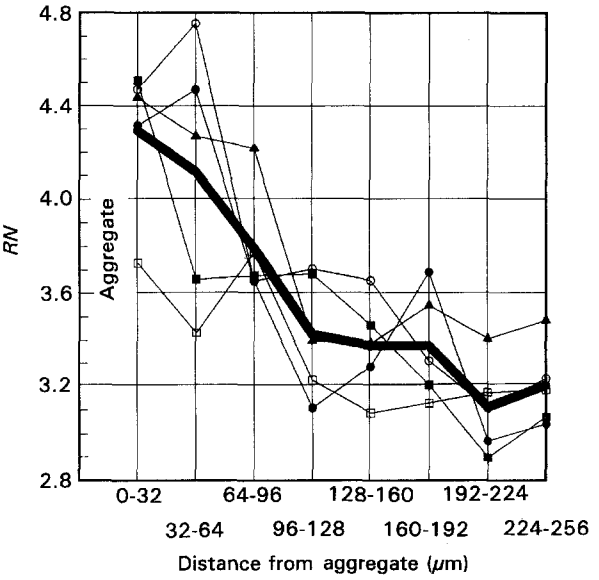

Figure 8 Plot of roughness number, *RN*, of the paste as a function of the distance from the aggregate particle. The *x*-axis represents the range of the surface region for which roughness was computed. (——) Average. Specimens: (●, ○) AA, (■, □) AB, (▲) AC.

gives an average spacing between particles that are equidistant in all directions. The surface to surface distances, *d*, are 2.00 mm (2000 μm), 1.12 mm (1120 μm), and 0.380 mm (380 μm) for specimens AA, AB, and AC, respectively. The particle spacing in

specimen AC, which contained the largest volume of aggregate, is large enough so that, on an average basis, there is no contribution of the interfacial zone on the roughness computations for the regions that were considered far away from the interface. The roughness of the bulk paste is distinguished from that of the paste–aggregate interface, and provides a basis for investigating the influence of the transition zone on the fracture of concrete.

3.2. Fracture toughness and its relationship to the paste roughness

A summary of the fracture parameters obtained from the TPFM and particle surface to surface spacing is given in Table III. The roughness number of the paste is related to K_{IC} in Fig. 9. The value of K_{IC}, a gauge of a material's resistance to crack propagation, increases with increasing roughness of the paste. The increase in paste roughness, associated with the increased paste–aggregate interfaces, increases the toughness of the paste and of concrete. Thus, the increase in toughness of the concrete beams may be attributed to a mechanism that induces roughening of the paste.

In order to gain a better understanding of the influence of the paste–aggregate interface on fracture toughness, a link should be made between the fracture parameters and the physical process of crack propagation. The advance of a crack from initiation to critical effective length, Δa_c, is controlled by the properties of the paste. In turn, the properties are related to microstructure which can be characterized by roughness. The ratio of the critical crack extension, Δa_c, to aggregate particle spacing, d, is indicative of the fraction of Δa_c that passed through the interface regions (which exhibit a higher roughness). Even though Δa_c did not change very much with the increase in roughness for specimens AA and AB (see Table III), Fig. 10 shows that the toughness (represented by K_{IC}) increased as the ratio $\Delta a_c/d$ increased. The increase in toughness can be explained by the graph in Fig. 11, which indicates that as the paste becomes rougher, due to the increased presence of the paste–aggregate interface, a higher fraction of the critical crack is in the interface.

TABLE III A summary of the fracture parameters evaluated from the two-parameter fracture model (TPFM) and the theoretical values of aggregate spacing

Specimen	K_{IC} ($N m^{-3/2}$)	Δa_c (mm)	$CTOD_c$ (mm)	Aggregate spacing (mm)
C	274000	2.43	0.00266	–
AA	376000	2.42	0.00373	2.00
AB	504000	2.57	0.00370	1.12
AC	774000	6.37	0.00813	0.38

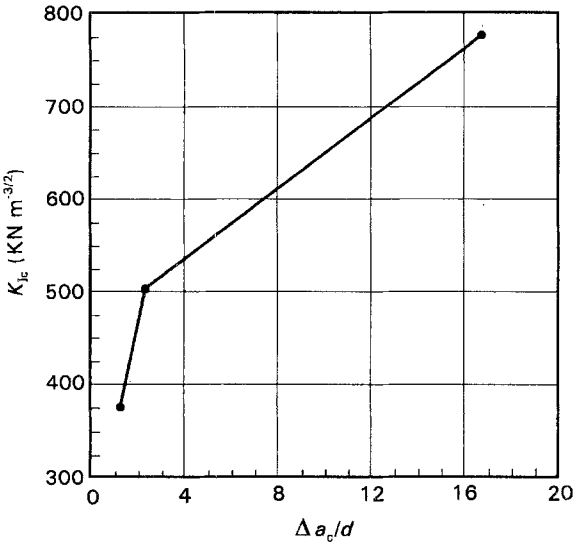

Figure 9 Graph of the average critical stress intensity factor, K_{IC}, as a function of roughness number, RN, of the paste.

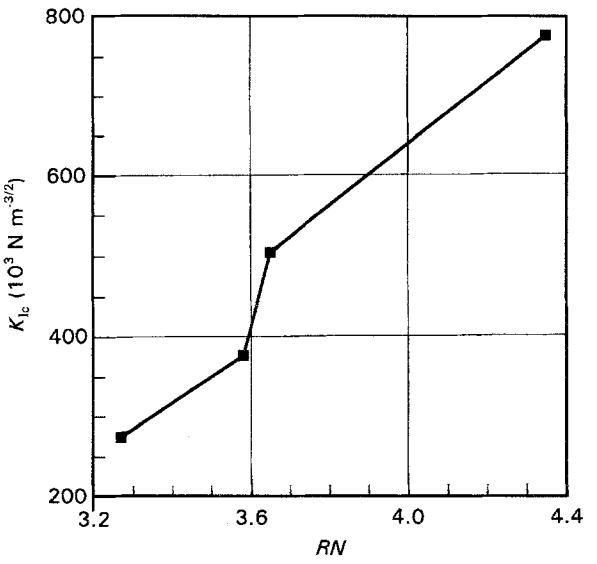

Figure 10 Graph of K_{IC} (critical stress intensity factor) as a function of $\Delta a_c/d$ (ratio of the critical effective crack extension to theoretical aggregate particle spacing).

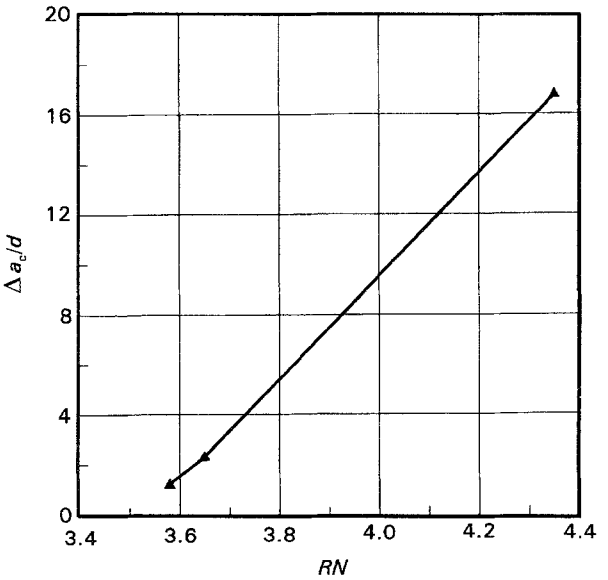

Figure 11 Plot of $\Delta a_c/d$ (ratio of the critical effective crack extension to theoretical aggregate particle spacing) as a function of the paste roughness.

In specimen AC, the spacing between aggregate surfaces is extremely small compared to Δa_c. Taking into consideration the size of the aggregate particles (which ranges between 4.75 and 2.36 mm), the critical crack length in specimen AC always results from the crack climbing around the aggregate. For specimens AA and AB (see Table III) one can conclude that the critical effective crack length may be reached without the crack climbing around the aggregate, because the critical effective crack length is only slightly larger, on average, than the smallest diameter of the aggregate particles, and smaller than the largest aggregate particle.

Fracture toughness for the specimens tested is dictated by the relative amount of interface present in concrete. As the aggregate content increases, the fracture process involves more interactions with the paste–aggregate interface. Thus, the increase in roughness with K_{IC} is indicative, at least in part, of the transition zone's increasingly dominant effect on the paste toughness.

4. Conclusions

The roughness of the paste fracture surface has been characterized as a function of varying amounts of pea gravel aggregate. Furthermore, the roughness of the paste increases as distance from the aggregate decreases. The roughness number, *RN*, approaches a value between 4.3 and 4.5 near the aggregate and gradually decreases to a value between 3.0 and 3.2 at distances greater than 100 μm from the aggregate – a value about the same as in the control specimen. This suggests that, as measured by *RN*, the transition zone is approximately 100 μm thick, which is in contrast to the previously reported values of 40–50 μm. Increasing the amount of aggregate increases the concentration of the paste–aggregate interface, thereby causing the average *RN* to shift upwards.

Microstructure and fracture toughness are found to be related. Fracture toughness parameters, as obtained from the TPFM, are in turn correlated to the roughness of the paste. Fracture of concrete is shown to be influenced by the roughness of the cement paste, which, in turn, is influenced by the presence of the paste–aggregate interface. The paste–aggregate interface toughens the paste by increasing its roughness.

Acknowledgements

The authors wish to thank the National Science Foundation (NSF) Center for Science and Technology of Advanced Cement-Based Materials (ACBM), Evanston, IL for supporting this research (Grant DMR, 9120002/03)

References

1. S. P. SHAH, in "Fracture Mechanics of Concrete: Dependence of Concrete Fracture Toughness on Specimen Geometry and on Composition", edited by A. Carpentieri and A. R. Ingraffea (Martinus and Nijhoff, The Hague 1984) p. 111.
2. S. MINDESS, in "Fracture Mechanics of Concrete: Fracture Toughness Testing of Cement and Concrete", edited by A. Carpentieri and A. R. Ingraffea (Martinus and Nijhoff, The Hague 1984) p. 67.
3. M. KACHANOV, in "Fracture Toughness and Fracture Energy of Concrete Interaction of a crack with some Microcrack Systems", edited by F. H. Wittman (Elsevier Science, Amsterdam, 1986) p. 3.
4. K. T. FABER and A. G. EVANS, *Acta Metall.* **31** (1983) 565.
5. J. G. M. van MIER, *Cem. Concr. Res.* **21** (1991) 1.
6. S. P. SHAH and C. OUYANG, *Trans. ASME* **15** (1993) 300.
7. J. FARAN, *Rev. Mater. Constr.* **490–491** (1956) 155. **492** (1956) 191.
8. *Idem. ibid.*
9. B. D. BARNES, SIDNEY DIAMOND and W. L. DOLCH, *J. Am. Ceram. Soc.* **76** (1979) 24.
10. L. STRUBLE, J. SKALNY and S. MINDESS, *Cem. Concr. Res.* **10** (1980) 277.
11. P. J. M. MONTEIRO and P. K. METHA, *ibid.* **15** (1985) 378.
12. P. J. M. MONTEIRO, J. C. MASO and J. P. OLLIVIER, *ibid.* **15** (1985) 953.
13. P. J. M. MONTEIRO and CLAUDIA O. OSTERTAG, *ibid.* **19** (1989) 987.
14. A. BENTUR, in Proceedings of the Conference on Advances in Cementitious Materials, Gaitherburg (MD), July 1990, edited by S. Mindess (The American Society, Westerville, OH, 1990) p. 523.
15. K. MITSUI, Z. LI, D. A. LANGE and S. P. SHAH, *ACI Mater. J.* **91** (1994) 30.
16. S. P. SHAH and F. O. SLATE, in "Proceedings of the International Conference on the Structure of Concrete", edited by (A. E. Brooks and K. Newman Cement and Concrete Association, London, 1965) p. 82.
17. X. PING and T. MINGSHU, *Il Cimento* **85** (1988) 33.
18. D. A. LANGE, H. M. JENNINGS and S. P. SHAH, *J. Am. Ceram. Soc.* **76** (1993) 589.
19. RILEM, *Mater. Construct.* **23** (1990) 461.
20. Y. JENQ and S. P. SHAH, *J. Eng. Mech.* **111** (1985) 1227.
21. D. A. LANGE, H. M. JENNINGS and S. P. SHAH, *J. Mater. Sci.* **28** (1994) 3879.
22. K. L. SCRIVNER, A. BENTUR and P. L. PRATT, *Adv. Cem. Res.* **1** (1988) 230.
23. LYBIMOVA, T. YU and PINUS, *Colloid J. USSR* **24** (1962) 491.

Received 25 April
and accepted 7 June 1994